Available at www.sciencedirect.com

ScienceDirect

journal homepage: www.elsevier.com/locate/he

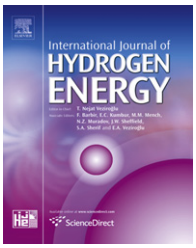

Efficiency of hydrogen internal combustion engine combined with open steam Rankine cycle recovering water and waste heat

Noboru Yamada [a,*], *Md Nor Anuar Mohamad* [b]

[a] *Graduate School of Energy and Environment Science, Nagaoka University of Technology, 1603-1 Kamitomioka, Nagaoka 940-2188, Japan*
[b] *Department of Mechanical Engineering, Nagaoka University of Technology, 1603-1 Kamitomioka, Nagaoka, Niigata 940-2188, Japan*

ARTICLE INFO

Article history:
Received 17 September 2009
Received in revised form
24 November 2009
Accepted 24 November 2009
Available online 8 December 2009

Keywords:
Hydrogen internal combustion engine
Waste heat recovery
Water recovery
Open Rankine cycle
Thermal efficiency
Combined cycle

ABSTRACT

A hydrogen internal combustion engine (HICE) wastes more heat, and producing nearly three times more water than a conventional engine. This paper describes the principle behind a novel waste heat recovery sub-system that exploits the water produced by an HICE as the working fluid for an open-cycle power generation system based on the Rankine cycle. Water from the HICE exhaust is superheated by the waste heat from the HICE and used to produce power in a steam expander. A fundamental thermodynamic model shows the contribution of the sub-system to the overall thermal efficiency of the HICE at various engine speeds, with and without a condenser. The results show that the condenser is not cost-effective and that the overall thermal efficiency with the proposed sub-system is 27.2% to 33.6%, representing improvements of 2.9% to 3.7%, at engine speeds of 1500 to 4500 rpm.

1. Introduction

Recently, the worldwide energy crisis and environmental issues have prompted vehicle manufacturers to produce vehicles with high energy efficiency using power generation processes that do not harm the environment. In the case of conventional internal combustion engines (ICEs), many studies on waste heat recovery sub-systems have been conducted to enhance the overall thermal efficiency. One of the most frequently used recovery sub-systems is a Rankine cycle, i.e., a steam power generation cycle [1,2]. There are two types of Rankine cycles: a closed Rankine cycle and open Rankine cycle. In an open Rankine cycle system, the working fluid is ejected from the system after it produces work output, while it is reused in the closed cycle. A classical locomotive steam engine is an example of a successful open Rankine cycle system. Although there are many types of working fluids for the Rankine cycle, water is one of the most desirable fluids in terms of safety, environmental friendliness, and thermodynamic characteristics at high temperatures and pressures [1].

The hydrogen internal combustion engine (HICE) is now being widely studied by many researchers because of its ability to mitigate the energy and environmental issues faced by the world. The ability of an HICE to run under bi-fuel or flex-fuel operating conditions [3] makes it possible for it to replace the present type of ICE with some modifications. If this

* *Corresponding author*. Tel./fax: +81 258 47 9762.
E-mail addresses: noboru@nagaokaut.ac.jp (N. Yamada), anuarm@stn.nagaokaut.ac.jp (M.N.A. Mohamad).
0360-3199/$ – see front matter © 2009 Professor T. Nejat Veziroglu. Published by Elsevier Ltd. All rights reserved.
doi:10.1016/j.ijhydene.2009.11.088

approach is realized, the investment cost for introducing HICEs into the automobile industry will be lower than the introduction of a completely new technology such as a "fuel cell" power train system. This is why the HICE is considered to be a promising candidate for future application to a vehicle power train system. At the same time, an HICE produces, not only waste heat, but also a large amount of water as a by-product of combustion. Based on low heating value of a fuel, an HICE emits nearly three times as much water per energy content, compared to a conventional ICE which runs on gasoline. This water would be a potentially valuable resource if it could be utilized for some useful purpose such as for the working fluid in a heat recovery system. For a power plant system, Sugishita et al. (1998) [4] reported simulation results for a closed hydrogen combustion turbine cycle that was powered by extracted steam from hydrogen combustion combined with a closed Rankine cycle as a bottoming cycle. Thus far, however, no research has been conducted on a recovery sub-system that recovers both waste heat and water from an HICE, especially in an automotive application.

In this study, we propose a new concept for a recovery sub-system for an HICE in an automotive application, and elucidate the efficiency of an HICE combined with the proposed recovery sub-system. An open steam Rankine cycle is employed as the power generation cycle of the recovery sub-system, which exploits the water exhausted from the HICE as its working fluid to convert the waste heat energy into power. We examine two designs of the fundamental thermodynamic model of the recovery sub-system and estimate the thermal efficiency of the recovery sub-system and the overall thermal efficiency of the entire system, including both the primary HICE and the recovery sub-system under various engine speed conditions for the HICE.

2. Hydrogen internal combustion engine

The HICE is considered to be a primary power generation system since it offers a feasible interim solution that utilizes the existing capital investment and technology more effectively than a fuel cell engine [5]. It is also considered to be a cost competitive and clean alternative to the conventional gasoline internal combustion engine [6]. Moreover, the use of hydrogen as a fuel offers the potential to contribute to the reduction of green house gases and local air pollution [7].

There are two important aspects regarding the HICE: it produces a large amount of water during its combustion process and the combustion temperature for hydrogen is higher than for gasoline [8]. The stoichiometric heat of combustion values per standard kg of air are 3.37 MJ and 2.83 MJ for hydrogen and gasoline, respectively [9]. The adiabatic flame temperature calculated using the Adiabatic Flame Temperature Program developed by C. Depcik [10] showed that the combustion temperature of hydrogen fuel was approximately 126 °C higher than that of gasoline fuel, when the combustion process occurred at $\lambda = 1$. The greatest issue for spark-ignited HICE combustion is the occurrence of a backfire and/or pre-ignition as the lean fuel/air ratio approaches the stoichiometric value, which limits the torque output of the engine [5]. The HICE power density, relative to gasoline operation, can be significantly below 83%, due to pre-ignition problems limiting the peak power output of the HICE [9]. Tang et al. (2002) [5] and Furuhama et al. (1978) [11] reported that pre-ignition limited the power density to 50% and 72%, respectively, relative to gasoline operation. A backfire occurs when a fresh charge of hydrogen is ignited in the intake ports, while pre-ignition occurs when the hydrogen charge is ignited after the intake valve closes but before the spark plug fires in the cylinder [12]. Both problems can be caused by the existence of a high temperature spot in the intake manifold or cylinder [9,12].

The above-mentioned aspects of an HICE inspired us to propose a new concept for a recovery sub-system that uses both the waste heat and water emitted from an HICE, to enhance its thermal efficiency. The proposed sub-system is expected to mitigate the high temperature spot problem by absorbing the undesirable excess heat from the HICE.

The following equation shows the HICE combustion process [13]:

$$2H_2 + \lambda O_2 + 3.76\lambda N_2 \rightarrow 2H_2O + (\lambda - 1)O_2 + 3.76\lambda N_2 \quad (1)$$

where λ denotes the ratio of the actual air quantity to the theoretical demand. The emissions produced by the HICE are, theoretically, only water and nitrogen gas when combustion is ideally carried out at a stoichiometric air-fuel ratio (AFR) of 34:1 with $\lambda = 1$, and other factors such as oxidation of the lubrication oil or the existence of other gases in the air are neglected. From Eq. (1), it is found that when 1 kg of hydrogen mass is supplied to the engine, approximately 9 kg of water are generated chemically by the combustion process at $\lambda = 1$. This seems to be enough water for the open steam Rankine cycle, which releases the water to the outside atmosphere after it is used to produce power. In an actual case, the air supplied to the HICE is humid; that is, the supplied air includes water vapor. Theil and Hartmann [14] of BMW reported detailed emissions data for an HICE using the hydrogen-balance method. From their results, it was estimated that the amount of water vapor emitted by the HICE was approximately 8.9 kg for 1 kg of hydrogen combusted for an actual driving distance of 100 km.

In addition, it is not always beneficial to have a large amount of water in the exhaust, since it affects, not only the exhaust system, but also any additional devices installed in the exhaust system. It is known that water vapor accelerates the corrosion of an exhaust pipe under a high temperature condition, which causes the carbon monoxide (CO) and carbon dioxide (CO_2) detectors to provide incorrect readings. Therefore, removing the water from the exhaust may contribute to the mitigation of these problems.

3. Overview of recovery sub-system

Fig. 1 shows a schematic of an HICE combined with an open steam Rankine cycle recovery sub-system. The sub-system is a bottoming cycle of the primary HICE, and consists of five main components: a water separator (5), tank (6), pump (8), evaporator (12), and expander (14). The sub-system was designed to separate the water emitted from the HICE (1)

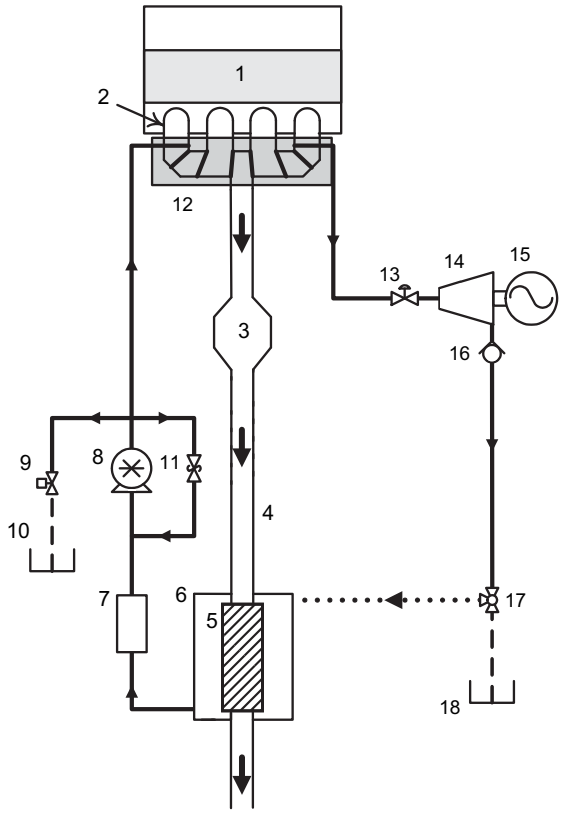

Component Description

1. HICE
2. Exhaust Manifold
3. Catalytic Converter
4. Exhaust Pipe
5. Water Separator
6. Tank
7. Water Filter
8. Pump
9. Power Valve
10. Drainage I
11. Relief Valve
12. Evaporator
13. Adjustable Valve
14. Expander
15. Electric Generator
16. Non-return Valve
17. 3-Way Valve
18. Drainage II

Line and Shape Description

Exhaust Flow
Flow Direction
Return Line

Fig. 1 – HICE system combined with open steam Rankine cycle recovery sub-system.

through its exhaust system (4) and utilize it as the working fluid of the open steam Rankine cycle. The separator (5), tank (6), and pump (8) are located after the catalytic converter (3) of the HICE, whereas the evaporator (12) is located on the exhaust manifold in order to extract high temperature waste heat. The expander (14) is located as close as possible to the evaporator to minimize the heat loss to the surroundings during the cycle operation. The water separator (5) and tank (6) are combined components, and are installed in the exhaust system (4) to separate the water from the exhaust gas of the HICE (1) and directly store the separated water in the tank (6). To maintain the function of the water separator (5), the separated water inside the tank should not be able to return to the exhaust system, which will continuously add water to the tank (6). A water filter (7) is installed before the pump (8) to remove contaminants from the separated water in the tank, because the untreated water inside the tank may contain contaminants in the form of gases, hydrocarbons, particulates, and other dissolved organic and inorganic matter. Since the water is continuously supplied to the recovery subsystem, there should be a mechanism to control the water level inside the tank, so that the amount of water is always at an optimum level. This can be done by a control system (not shown in Fig. 1) that allows any excess water to be drained to the atmosphere through drainage I (10). Here, power valve I (9) automatically opens and closes the drainage line based on the water level in the tank. A relief valve (11) is installed in parallel with the pump (8) to maintain the system pressure under the allowable pressure level. The water is delivered by the pump (8) to the evaporator (12) at the designated pressure and mass

flow rate. In the evaporator (12), the water temperature increases to a high temperature level according to the exhaust gas temperature at a constant pressure and then becomes superheated vapor. This superheated vapor is converted into rotation power when it expands in the expander (14). Low-pressure vapor leaving the expander (14) is released to the atmosphere via (16), (17), and (18) or is condensed by a condenser (not shown in Fig. 1) before being released to the atmosphere via (16), (17), and (18). A non-return valve (16) is installed after the expander (14) as a safety valve for unexpected conditions and to prevent atmospheric pressure or high-pressure exhaust gas from entering the recovery system. A 3-way valve (17) is installed before drainage II (18) as an automatic switch for the system, which allows the water to be directed through drainage II (18) or returned to the tank (6) if an insufficient amount of water is detected for the next cycle operation. This type of operation is called semi-closed Rankine cycle operation hereafter. Since the load condition, i.e., the engine speed of the HICE, varies based on driving conditions, the mass flow rate of the HICE exhaust gas and its temperature also vary accordingly. Therefore, the control system plays the important role of ensuring the smooth operation of the recovery sub-system. The control system should perform the following operations:

- Detect and maintain the water level inside the tank (6), and enable the recovery sub-system to operate only when an appropriate water level and quantity of separated water are detected. This can be done by the semi-closed Rankine cycle operation.
- Only allow an appropriate amount of water to be pumped to the evaporator (12) so that the water can evaporate at the designated temperature when it is heated by the available heat inside the evaporator. This can be done by controlling the mass flow rate of the water through the pump (8).
- Only allow steam at an appropriate pressure to enter the expander. This control can be achieved by installing an adjustable valve (13) before the expander (14).

The power produced by the expander (14) is used to drive an electrical generator (15). The generated electric power could be utilized in many ways, such as being directed to a battery, driving electrical devices, or for other purposes. The separation of water from the exhaust gas in the water separator (5) is one of key processes of the proposed sub-system. However, the design details for this water separator were not discussed in this study. Interesting designs for water separators have recently been proposed by some inventors [15–17]. One example is the inertial water separator. In this study, it was assumed that the water separator performs its separation with an efficiency of 50%, as mentioned later, and that the water separator does not consume power.

4. Simulation model and method

The objectives of the present simulation were to elucidate the thermal efficiency of the recovery sub-system, to show whether the recovery sub-system has the potential to contribute to the overall thermal efficiency of the entire system, and to determine whether a sufficient amount of working fluid (water) could be recovered by the water separator to recover the heat wasted through the HICE exhaust system.

Fig. 2 shows a simulation model of the open steam Rankine cycle recovery sub-system. The layout of the main components is similar to Fig. 1 and each link between the components is marked with a number representing the state of the working fluid. Here, the condenser and electric fan inside the

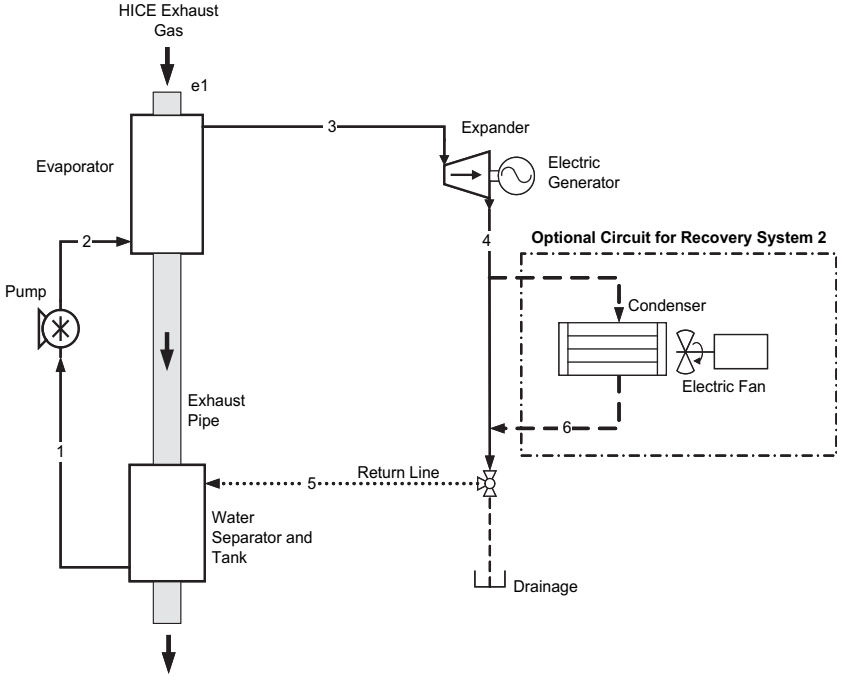

Fig. 2 – Simulation model of open steam Rankine cycle recovery sub-system.

enclosed dashed–dotted line represent an optional configuration for recovery sub-system II (RS–II). The electric fan is incorporated with the condenser to enhance the heat transfer from the condenser to the ambient air. The system without the condenser is hereafter called recovery sub-system I (RS–I), whereas the system with the condenser (and electric fan) is called RS–II. The solid line with the arrows in Fig. 2 represents the flow direction of the working fluid for RS–I, whereas the dashed line represents the flow direction modification for RS–II. The working fluid in RS–II flows through the dashed line into the condenser before it is drained or directed to the tank. The condenser in RS–II was installed to elucidate its effect on the thermal efficiency of the recovery sub-system and the overall thermal efficiency of the entire system since a condenser is generally employed in a conventional closed steam Rankine cycle to reduce the pressure at the expander outlet, and to increase the thermal efficiency of the cycle.

In this study, the HICE conditions, engine power, total combustion heat, and brake thermal efficiency of the engine, were calculated as follows [18,19]:

$$W_{HICE} = 2\pi\omega\Gamma \times 10^{-3} \tag{2}$$

$$Q_{total} = \dot{m}_f Q_{LHV} \tag{3}$$

$$\eta_{BTE} = \frac{W_{HICE}}{Q_{total}} = \frac{W_{HICE}}{\dot{m}_f Q_{LHV}} \tag{4}$$

where ω is the angular speed of the HICE in revolutions per second (rps), Γ is the HICE brake torque in Nm, $\dot{m}_f$ is the mass flow rate of the supplied fuel in kg/s, and Q_{LHV} is the lower heating value of the fuel in kJ/kg. For the hydrogen, $Q_{LHV} = 120 \times 10^3$ kJ/kg. Hereafter, all of the units for power and heat will be expressed in kW, temperature in °C, mass flow rate in kg/s, enthalpy in kJ/kg, and entropy in kJ/kg K. It should be noted that "brake thermal efficiency" is a technical term often used in engine performance evaluation. It has the same definition as the overall thermal efficiency or fuel conversion efficiency of an engine [19], since it represents some percentage of fuel converted into useful work (i.e., engine power).

In the case of the recovery sub-systems, the efficiencies of the main components [20]—the water separator, expander, pump, heat exchanger, and electric generator—are explicitly given as shown in Table 1. The water separator efficiency is defined by the following equation:

Table 1 – Efficiencies for recovery sub-system components.

Component	Efficiency
Water separator[a]	$\eta_s = 50\%$
Pump[b]	$\eta_p = 60\%$
Expander[b]	$\eta_E = 70\%$
Electric generator[a]	$\eta_G = 85\%$
Heat exchanger[a]	$\eta_{HX} = 80\%$

a Estimated data.
b Data was taken from Chammas and Clodic (2005).

$$\eta_s = \frac{\dot{m}_{sw}}{\dot{m}_T} \tag{5}$$

where $\dot{m}_{sw}$ is the mass flow rate of the separated water and $\dot{m}_T$ is the mass flow rate of the total amount of water in the HICE exhaust gas before the separation process. The efficiencies of the expander and pump are defined as:

$$\eta_E = \frac{h_3 - h_{4a}}{h_3 - h_{4s}} \tag{6}$$

$$\eta_p = \frac{h_{2s} - h_1}{h_{2a} - h_1}, \tag{7}$$

respectively, where h is the enthalpy of the working fluid. The subscripts a and s for the enthalpy refer to actual (non-isentropic) and ideal (isentropic) processes, respectively. The subscript numbers correspond to the numbers in Fig. 2.

The electric generator efficiency is defined as:

$$\eta_G = \frac{W_G}{W_E} \tag{8}$$

where W_G is the generated electric power and W_E is the power converted by the expander. When the heat loss from the heat exchanger to the surroundings is negligible, the performance of heat exchanger is represented by its effectiveness. The effectiveness is defined as the ratio of the actual rate of heat transfer by the heat exchanger to the maximum possible heat transfer rate between the fluids [21–24]. Therefore, in this study we use

$$\varepsilon = \frac{T_3 - T_{2a}}{T_{e1} - h_{2a}} \tag{9}$$

where ϵ is the heat exchanger effectiveness and $\epsilon = 0.8$ is assumed in the simulation. T_{e1} is the temperature of the HICE exhaust gas entering the evaporator, whereas T_{2a} and T_3 are the temperature of water at evaporator inlet and outlet, respectively. The energy balance in the evaporator is conserved by the following equations:

$$Q_{evap} = Q_{exh} - Q_{ew} \tag{10}$$

$$Q_{evap} = \frac{Q_{in}}{\eta_{HX}} = \frac{\dot{m}_w(h_3 - h_{2a})}{\eta_{HX}} \tag{11}$$

where Q_{evap} is the portion of the HICE exhaust waste heat that passes through the evaporator and is used as a heat source for the recovery sub-system, $\dot{m}_w$ is the mass flow rate of the working fluid (water) controlled by the pump, η_{HX} is the heat exchange efficiency of the evaporator, Q_{in} is the heat that the working fluid gains at the evaporator, Q_{exh} is the HICE exhaust waste heat (i.e., the heat of the HICE exhaust gas), and Q_{ew} is the heat leaving the HICE exhaust gas before the gas reaches the evaporator. In this study, $Q_{ew} = 0.2 \times Q_{exh}$ is assumed.

The generated electric power is calculated as:

$$W_G = \dot{m}_w \eta_G (h_3 - h_{2a}). \tag{12}$$

The pump power is calculated as:

$$W_P = \dot{m}_w (h_{2a} - h_1). \tag{13}$$

The net thermal efficiencies of RS–I and RS–II can then be calculated using:

$$\eta_{th} = \frac{W_G - W_P}{Q_{in}}. \quad (14)$$

The net power values for RS–I and RS–II are respectively defined as follows:

$$W_{RS-I} = W_G - W_P \quad (15)$$

$$W_{RS-I} = W_G - W_P - W_C \quad (16)$$

where W_C is the electric power consumption of the electric fan incorporated with the condenser (we will call it the ''condenser fan power'' hereafter) in RS–II. Finally, the total power and overall thermal efficiency of the entire system are given by:

$$W_{total} = W_{HICE} + W_{RS-I}, \quad \text{or} \quad W_{total} = W_{HICE} + W_{RS-II} \quad (17)$$

$$\eta_{overall} = \frac{W_{total}}{Q_{total}} \quad (18)$$

where Q_{total} is the total heat provided by the hydrogen combustion in the HICE, as defined by Eq. (3).

The simulation work in this study began by analyzing the HICE conditions by extracting the engine parameters from the available published data on HICEs. Verhelst et al. [3] reported that a four-cylinder sixteen-valve engine with a displacement volume of 1783 cc, running on hydrogen fuel, has brake thermal efficiencies, η_{BTE}, that are relatively higher than when it runs on gasoline fuel at a specific brake torque, Γ. Table 2 shows the selected engine experimental conditions for this study taken from their experiments. Based on their data for the η_{BTE} at $\Gamma = 40$ Nm, with an engine running on hydrogen fuel under stoichiometric conditions, the W_{HICE} and $\dot{m}_f$ values can be estimated using Eqs. (2) and (4), respectively, at various engine speeds. From Eq. (3), Q_{total} can be estimated after the value of $\dot{m}_f$ is known. Due to the absence of available data for the heat balance of an HICE, the Q_{exh} of the HICE was assumed from the data for a gasoline/hydrogen mixed fuel engine [25]. Yüksel and Ceviz observed that the heat loss through the exhaust gas of a four-cylinder engine with a 1796 cc displacement volume burning a gasoline/hydrogen mixed fuel was nearly the same as when it operated on pure gasoline. Based on their percentage value data for the heat loss through the exhaust gases at various engine speeds, the same percentage was assumed for Q_{exh} in this study. The selected engine experimental conditions for this analysis taken from their experiment are shown in Table 3. The other energy fractions, i.e., Q_{total} and W_{HICE}, were taken directly from the Verhelst et al. [3] study, whereas the other unspecified energy fraction (consisting of cooling and other losses) was estimated by subtracting all of the known energy fractions from Q_{total}. Fig. 3 shows the HICE energy fractions, which included the HICE exhaust waste heat Q_{exh}, engine power W_{HICE}, and other unspecified heat losses (these are called ''HICE cooling and other losses'' hereafter).

Fig. 4 shows the exhaust gas temperatures of the HICE at the evaporator inlet and outlet for various engine speeds. The data for the HICE exhaust gas temperatures at the exhaust manifold, T_{e1}, reported by Verhelst et al. [3] at 3500 rpm and 4500 rpm were used. Based on their data, the temperature variation was assumed to be linear with the engine speed. The recovery sub-system was assumed to be ideally insulated, so that there was no heat loss through the system boundaries, such as pipes, component walls, etc.

Fig. 5 shows the mass flow rates for the fuel (Hydrogen) consumption, $\dot{m}_f$, total amount of water, $\dot{m}_T$, and separated water, $\dot{m}_{sw}$, from the HICE exhaust gas for various engine speeds. The $\dot{m}_T$ values were calculated from Eq. (1) by assuming $\lambda = 1$, and the mass flow rate for the separated water, $\dot{m}_{sw}$, was calculated from Eq. (5) by assuming $\eta_s = 50\%$. The required mass flow rate of the working fluid water, $\dot{m}_w$, varied with the engine speed ($\dot{m}_w$ is shown in Fig. 10). For continuous operation of the proposed sub-system, the value of $\dot{m}_w$ should be less than that of $\dot{m}_{sw}$ in the case without the semi-closed Rankine cycle operation (i.e., open steam Rankine cycle operation).

Fig. 6(a) and (b) shows a temperature–entropy (T–s) diagram of the simulated open Rankine cycles of RS–I and RS–II, respectively. The cycles for three representative engine speeds are shown: the lowest speed (1500 rpm), average speed (3000 rpm), and highest speed (4500 rpm). The state numbers correspond to the numbers shown in Fig. 2. In the calculation of the thermal property of water as the working fluid, the water was assumed to be pure water, and the thermal property was calculated by using the REFPROP refrigerant database version 8.0 [26]. There are two conditions at the expander outlet point, 4*a* and 4*s*, which represent the points achieved by actual (non-isentropic) and ideal (isentropic) expansions in the expander, respectively. The dashed lines represent the isentropic expansion processes for reference. These isentropic expansion processes occur only when the expander isentropic efficiency $\eta_E = 100\%$. Although the pump outlet

Table 2 – Selected engine condition taken from experiment by Verhelst et al. [3].

Engine experimental condition	Data
Engine type	Volvo (with CVVT), fuel injected
Fuel used	Hydrogen
Number of cylinders	4
Compression ratio	10.3:1
Displacement volume	1783 cc
Air fuel ratio, λ	1 (fixed)
Engine brake torque, Γ	40 Nm (fixed)
Engine speed	1500 ~ 4500 rpm

Table 3 – Selected engine condition taken from experiment by Yüksel and Ceviz [25].

Engine experimental condition	Data
Engine type	Ford MVH-418, fuel injected
Fuel used	Hydrogen–gasoline (mixed)
Number of cylinders	4
Compression ratio	10: 1
Displacement volume	1796 cc
Air fuel ratio, λ	0.8 ~ 1.1 (varies)
Engine brake torque, Γ	100 ~ 157 Nm (varies)
Engine speed	1500 ~ 4500 rpm

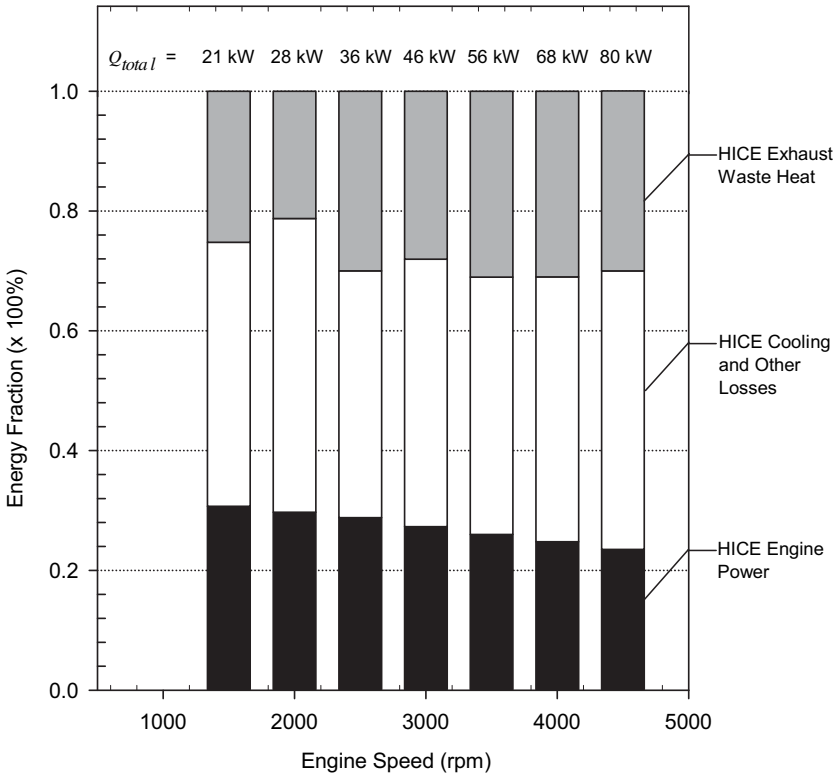

Fig. 3 – Energy fractions of HICE without recovery sub-systems for various engine speeds [3,25].

point (2) should also be shown in both the non-isentropic and isentropic compressions, these were merged into one point since their occurrence points were too close together to distinguish in this figure. The actual outlet points of the expander and pump were calculated, respectively, from Eqs. (6) and (7). For RS–I, the simulation process was ended at the isentropic expander outlet condition point 4*a*, whereas for RS–II it was ended at point 5 (condenser outlet).

For RS–I, the expander outlet pressure, P_4, was assumed to be an atmospheric pressure of 101.3 kPa. The separated water temperature, T_1, was assumed to be 65 °C (338.15 K), making it less than the dew point of the water vapor in the HICE exhaust gas. Considering the pressure resistance limitation of the material for recovery sub-systems, the maximum operating pressure for the expander inlet, P_3, (equal to pump pressure

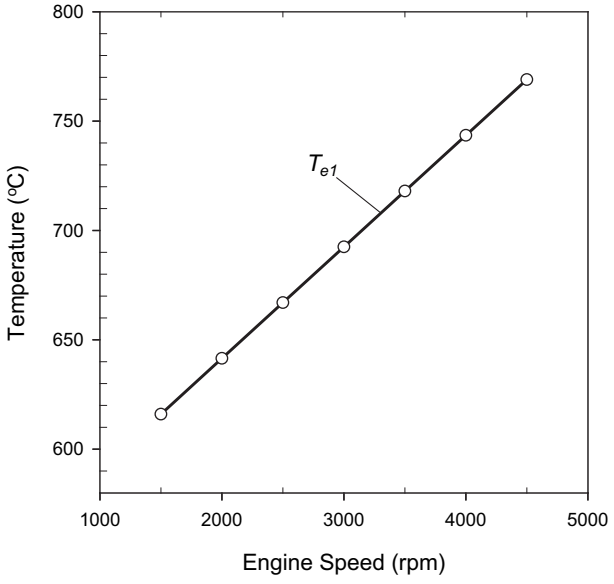

Fig. 4 – HICE exhaust gas temperatures at evaporator inlet (T_{e1}) for various engine speeds [3].

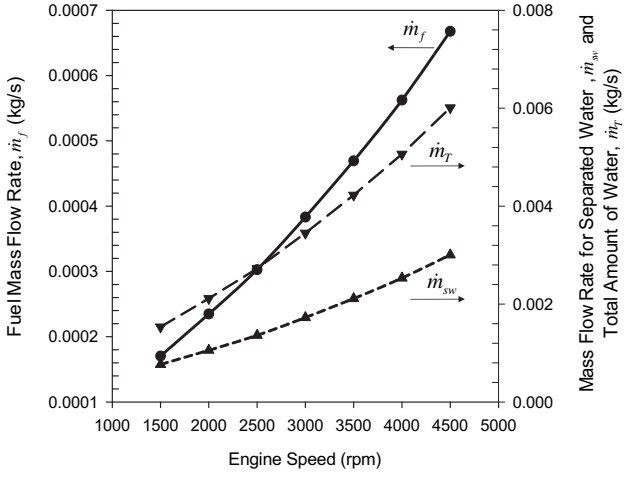

Fig. 5 – Mass flow rates of fuel (Hydrogen) consumption, total amount of water, and separated water for various engine speeds.

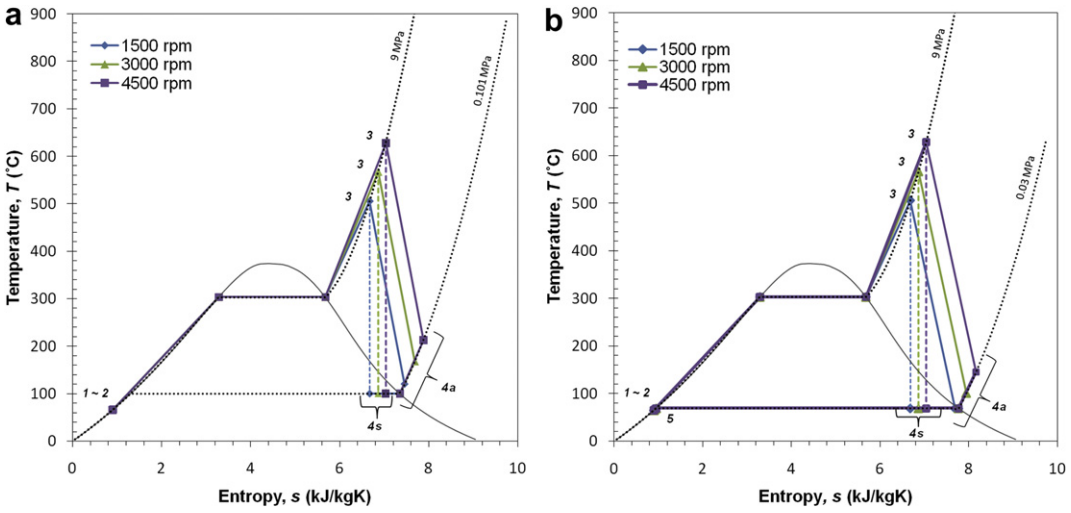

Fig. 6 – Simulated open Rankine cycle of recovery sub-system at low, average, and high engine speed conditions. (a) RS–I; (b) RS–II.

P_{2s}) was limited to 9 MPa [1]. The minimum temperature level in this study was larger than the critical temperature of water (i.e., 373.95 °C), thus enabling the recovery sub-system to operate at the maximum pressure level of 9 MPa even at 1500 rpm, since the fluid condition at the expander inlet was prevented from falling into the wet region. From REFPROP, the fluid properties at the pump outlet, s_{2s}, T_{2s}, and h_{2s}, were also estimated at $P_{2s} = P_3$. From h_1 and h_{2s}, the value of h_{2a} was calculated using Eq. (7). Using REFPROP again, T_{2a} was estimated at $P_{2a} = P_3$ and h_{2a}, and T_3 was calculated from Eq. (9). Finally, from T_3 and P_3, h_3 was estimated from REFPROP, and the other parameters, Q_{evap} and $\dot{m}_w$, were calculated from Eqs. (10) and (11), respectively.

For RS–II, the T_3 value for each engine speed was the same as that for RS–I. However, the P_4 and T_4 values were assumed to be lower than those of RS–I because the condenser lowered the value of P_3. The RS–II process ended at point 5, as shown in Fig. 2. At point 5, all of the water vapor was assumed to be condensed into saturated liquid water. Thus, in RS–II, a lower expander outlet pressure and higher expansion ratio are basically expected. As a result, a higher enthalpy difference can be reached, higher electric power, W_G, can be generated, and a higher thermal efficiency, η_{th}, can be achieved compared to RS–I. For RS–II, an expander outlet pressure of 30 kPa for all engine speeds was assumed by expecting the water temperature can be reduced in condenser to 70 °C. A condenser fan power consumption of 0.2 kW was also assumed based on average motor power consumption for radiator fan with outside diameter range from 280 mm to 400 mm.

5. Results and discussion

Fig. 7 shows the thermal efficiencies of RS–I and RS–II. Fig. 8 shows the overall thermal efficiencies of the entire system, comparing the use of RS–I or RS–II with the case without a recovery sub-system. RS–II had a higher thermal efficiency than RS–I. For the thermal efficiency of RS–I, $\eta_{th} = 18.2\%$ to 19.5% for lower to higher HICE engine speeds, whereas for the thermal efficiency of RS–II, $\eta_{th} = 21.5\%$ to 22.7% for the same engine speeds. However, as shown in Fig. 8, the overall thermal efficiencies, $\eta_{overall}$, of the HICE combined with the two recovery sub-systems were comparable. The $\eta_{overall}$ values for the two designs approximately overlapped, with values ranging from 27.2% to 33.6% for engine speeds of 1500 rpm to 4500 rpm. RS–II had a slightly higher overall thermal efficiency than RS–I, except at speeds lower than 2500 rpm. As compared to the HICE without a recovery sub-system, the increase in $\eta_{overall}$ by RS–I varied from 2.9% to 3.7% in the range of 1500 rpm to 4500 rpm.

Fig. 9 shows the net power, pump power, and condenser fan power of RS–I and RS–II, along with the HICE engine power, for various engine speeds. It can be seen that the net power of RS–II (W_{RS-II}) was comparable to that of RS–I (W_{RS-I}) because the amount of pump power (W_P) and condenser fan power (W_C) consumed in RS–II was more than four times the pump

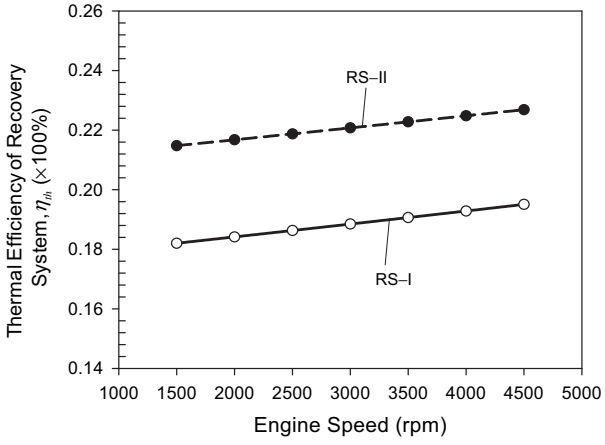

Fig. 7 – Thermal efficiencies of RS–I and RS–II for various engine speeds.

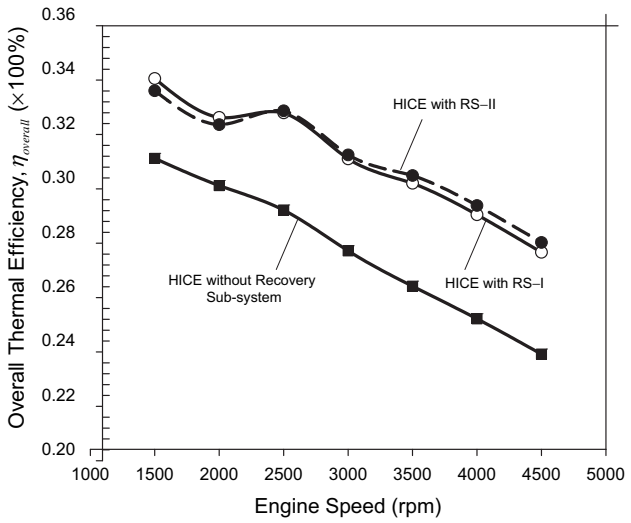

Fig. 8 – Overall thermal efficiencies of HICE combined with RS–I and RS–II for various engine speeds.

power consumed in RS–I. This resulted in comparable $\eta_{overall}$ values for RS–II and RS–I, even though RS–II had a higher η_{th} than RS–I. The value of W_{RS-II} fell to approximately 0.09 kW at 1500 rpm due to relatively large values for W_P and W_C, as compared to W_{RS-I}.

From the above results, it can be concluded that under a constant engine torque particularly at 40 Nm, RS–I is the better choice when considering the cost effectiveness, smaller system design and comparable performance compared to RS–II. For the entire engine speed investigated in this study, RS–I contributed almost as much to $\eta_{overall}$ as RS–II. The authors reiterate that the proposed concept is unique for hydrogen combustion prime movers, and could be applied not only to an HICE but also to other hydrogen combustion power generation systems such as a hydrogen gas turbine system.

Fig. 10 shows a stack chart of the mass flow rates of the separated water, $\dot{m}_{sw}$, assuming a water separator efficiency, η_s, of 50%, along with the amount of additional water required $(\dot{m}_{required})$ to reach $\dot{m}_w(\dot{m}_w = \dot{m}_{sw} + \dot{m}_{required})$. From Fig. 10, the amount of $\dot{m}_{sw}$ is unable to supply 100% of the water required by the recovery sub-systems. Furthermore, there is a possibility that the water produced by an HICE under actual operating conditions may be lower than that under the theoretical stoichiometric conditions. This problem can be solved by the semi-closed Rankine cycle operation. In the present simulation model, the HICE operated at a low load condition (50% throttle position). Therefore, the HICE engine power, W_{HICE}, and its fuel consumption, $\dot{m}_f$, were small. This is why the amount of water produced by HICE, $\dot{m}_{sw}$, was small in this study. The recent progress in HICE development shown there are possible to run HICE at higher load condition using several methods [5,27–32]. Therefore, if this recovery sub-system is designed for an HICE that is capable of operating under a high load condition, more water could be recovered compared to present study. Of course, the water separator efficiency is also critical for the water recovery from HICE exhaust gas. An extremely high separator efficiency is not expected because it might aggravate the flow resistance of the exhaust.

In addition, Fig. 11(a) and (b) shows the predicted energy fractions of the entire system with RS–I and RS–II, respectively, as compared with Fig. 3. These figures allow us to compare the fractions of heat, power, and loss for an HICE

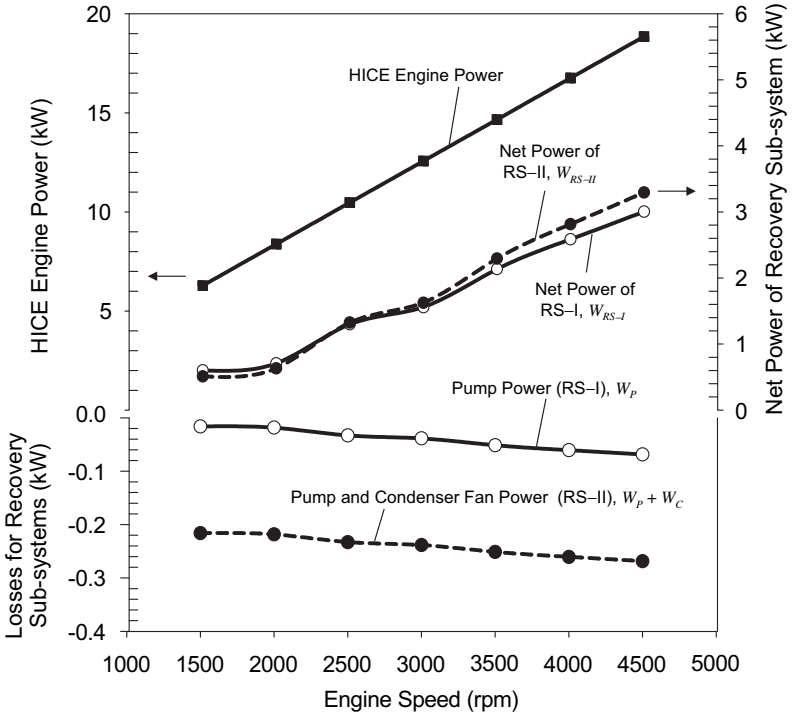

Fig. 9 – Net power, pump power of RS–I, pump and condenser fan power of RS–II, and HICE engine power for various engine speeds.

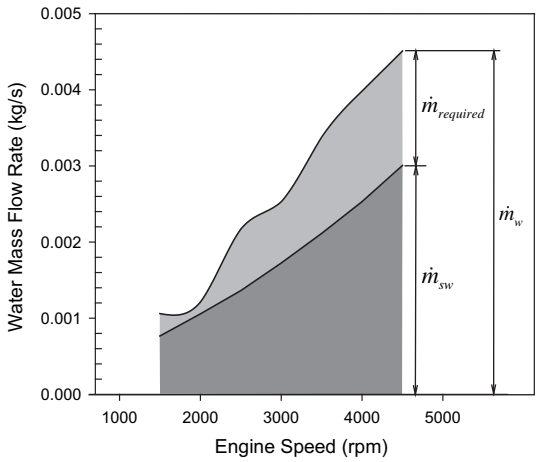

Fig. 10 – Water utilization by recovery sub-system for various engine speeds.

with RS–I, HICE with RS–II, and HICE without a recovery sub-system. The value of Q_{total} for each engine speed is presented at the top of each bar-graph, and Q_{total} is regarded as 100% of the energy fractions of the entire system. Q_{total} is broken down into the following fractions: the HICE engine power, HICE cooling loss, other HICE losses, and HICE exhaust waste heat. These fractions were assumed to be constant for either recovery sub-system. A certain percentage of the HICE exhaust waste heat, Q_{evap}, was then transferred to the recovery sub-system as Q_{in}, as defined by Eq. (11). Q_{in} is further broken down into the following fractions: electric power generated, electric generator loss, and waste heat. It should be noted that the W_P in RS–I, and $W_P + W_C$ in RS–II must by treated as power losses; therefore, the value of HICE engine power shown in Fig. 11 is the value after these losses have been deducted from the pure HICE engine power.

It is obvious that the ''cooling and other losses'' energy fraction is the largest energy fraction for the HICE. If this energy fraction is combined with the HICE exhaust waste, Q_{exh}, they account for approximately 70% to 77% of the total waste energy in the HICE for an engine speed range of 1500 rpm to 4500 rpm. The BMW corporation recently reported a dual Rankine cycle heat recovery system that utilizes, not only the exhaust waste heat, but also the cooling waste heat of a gasoline internal combustion engine. They discussed several heat exchanger configurations for efficient recovery [2]. On the other hand, realizing the fact that the exhaust gas temperature is largely influenced by fuel type, ignition timing, and valve timings, Shudo et al. [33] reported that a large heat loss occurs because the higher burning velocity and shorter quenching distance of hydrogen, as compared to other hydrocarbon fuels, increase the heat transfer from the burning gas to the combustion chamber wall. He also reported that the exhaust temperature for an engine fueled with hydrogen is lower than a similar engine fueled with methane at 1500 rpm with $\lambda = 1$ [34].

Considering these facts, it is probable that the heat and temperature levels are different from what have been assumed in this study. Thus, Figs. 12 and 13 are presented to show the effect of changes in the heat and temperature levels on the recovery sub-system performance. Fig. 12 shows the potential for overall thermal efficiency improvement when

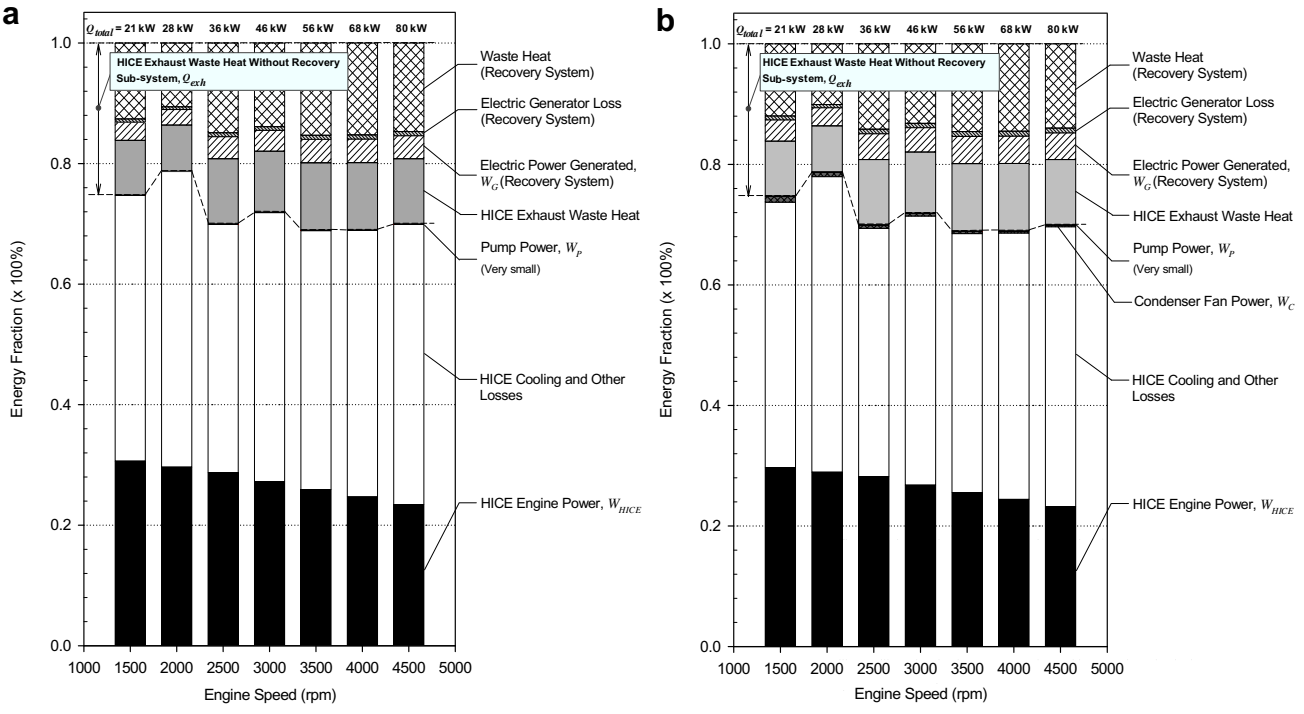

Fig. 11 – Energy fractions of HICE combined with the recovery sub-system for various engine speeds. (a) HICE with RS–I; (b) HICE with RS–II.

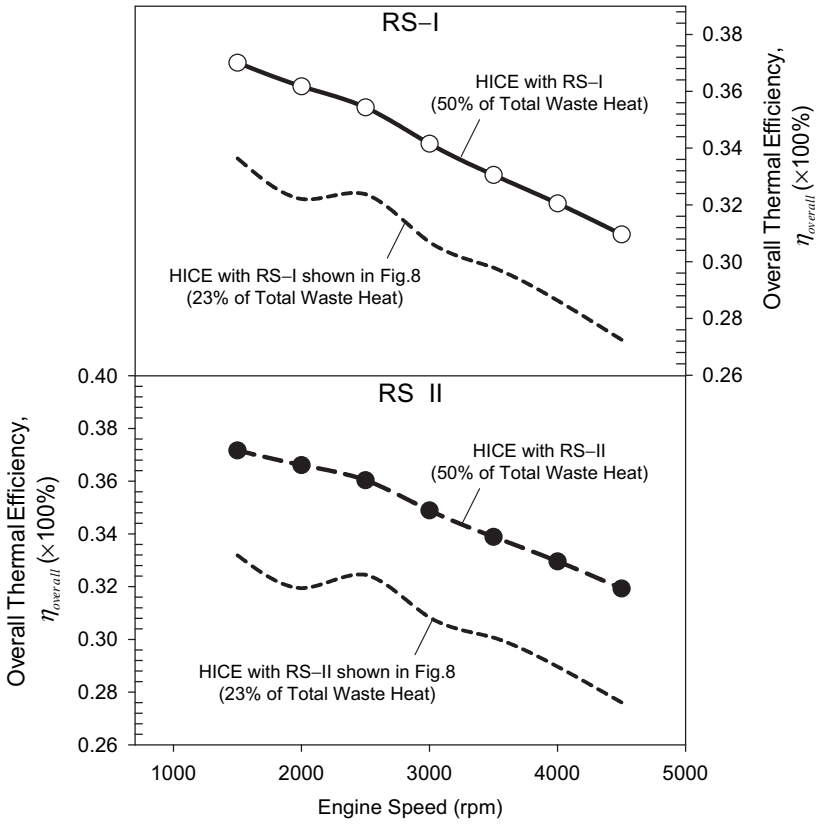

Fig. 12 – Potential for overall thermal efficiency improvement of the HICE when the recovery sub-systems recover 50% of the total wasted energy: RS–I and RS–II for various engine speeds.

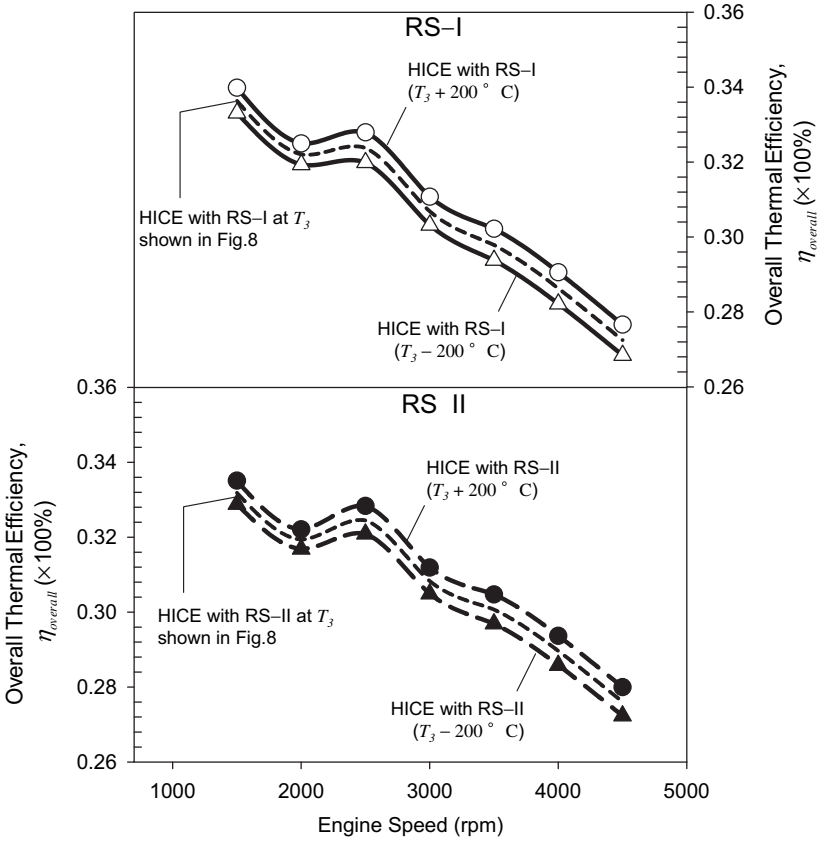

Fig. 13 – Trend of the overall thermal efficiency when the temperature of the expander inlet, T_3, is increased and decreased by 200 °C: RS–I and RS–II for various engine speeds.

50% of the total waste energy is able to be recovered by the recovery sub-systems, as compared to that shown in Fig. 8 when 23% of the total waste energy was recovered (i.e., the heat into the recovery sub-system Q_{in} becomes approximately double that used to obtain the value in Fig. 8). Fig. 13 shows the trend of the overall thermal efficiency when the temperature of the heat source at evaporator inlet T_3 is increased and decreased by 200 °C as compared to the value described in Fig. 4.

Fig. 12 indicates that an increase in Q_{in} will increase $\eta_{overall}$. The $\eta_{overall}$ varies from 6.3% to 7.5% for RS–I, and from 6.5% to 8.4% for RS–II for an engine speed range of 1500 rpm to 4500 rpm. These efficiencies are on average approximately 3.5% and 4% higher than the $\eta_{overall}$ shown in Fig. 8 for RS–I and RS–II, respectively, over all engine speeds. Fig. 13 indicates that $T_3 \pm 200$ °C results in $\eta_{overall} \pm 0.4\%$ for RS–I, and $\eta_{overall} + 0.4/-0.3\%$ for RS–II, averaging across the entire range of engine speeds. The increase in $\eta_{overall}$ from the value without any recovery sub-system is from 3.3% to 4.2% for RS–I, and from 2.8% to 4.5% for RS–II, when T_3 is increased by 200 °C, while a smaller change is obtained when T_3 is decreased by 200 °C, where the increase ranges from 2.6% to 3.3% for RS–I, and from 2.2% to 3.7% for RS–II, for an engine speed range of 1500 rpm to 4500 rpm. In this case, the difference in the required amount of water results in $\dot{m}_w + 3.4 \times 10^{-4}/-5.2 \times 10^{-4}$ kg/s on average over the entire range of engine speeds.

In this study, the simulation results imply that the proposed waste heat recovery sub-system will contribute to the overall thermal efficiency of an HICE, and that the sub-system can utilize the water recovered from the HICE exhaust gas, even though semi-closed Rankine cycle operation has to be considered. Furthermore, utilizing the waste heat, especially from an HICE cylinder, intake port, and manifold, will not only be useful, allowing the recovery sub-systems to maximize the Q_{in}, but might also contribute to an improvement in the HICE operation itself. If the pre-ignition and backfire problems can be solved by removing the heat from a hot spot in the HICE cylinder, intake port, or manifold, combining an HICE with a waste heat recovery sub-system will be an effective and beneficial way to improve the operational and thermal efficiency of the HICE.

6. Conclusions

An open steam Rankine cycle waste heat recovery sub-system combined with an HICE was newly proposed to recover both waste heat and water from the HICE. The recovery sub-system designs, one without a condenser (recovery sub-system I: RS–I) and the other with a condenser (recovery sub-system II: RS–II), were modeled and first-order simulations were carried out under various HICE engine speed conditions expected in an automobile application. The results of this study revealed the following:

1. Although the recovery sub-system with a condenser (RS–II) showed a slightly higher thermal efficiency than the recovery sub-system without a condenser (RS–I), both designs resulted in comparable overall thermal efficiencies for the entire system. Thus, in terms of cost effectiveness and small system design, RS–I is a better choice than RS–II.
2. RS–I showed a thermal efficiency that ranged from 18.2% to 19.5%, and an HICE combined with RS–I showed an overall thermal efficiency that ranged from 27.2% to 33.6%, which are 2.9% to 3.7% higher than that of a conventional HICE without any recovery sub-system in the engine speed range of 1500 rpm to 4500 rpm.
3. The water consumption in the recovery sub-system exceeded the amount produced by the water separator at a separator efficiency of 50%. Hence, a water collection process such as a semi-closed Rankine cycle operation has to be considered for continuous operation. Further research on water separators must be conducted for the realization of the proposed system.
4. Averaging the HICE engine speeds of 1500 rpm to 4500 rpm, an expander inlet temperature of $T_3 \pm 200$ °C resulted in an overall thermal efficiency of $\eta_{overall} \pm 0.4\%$ for RS–I, and $\eta_{overall} + 0.4/-0.3\%$ for RS–II, and a required amount of water of $\dot{m}_w + 3.4 \times 10^{-4}/-5.2 \times 10^{-4}$ kg/s for the working fluid of the recovery sub-system.

In the future, we will focus on research and development of an actual open steam Rankine cycle sub-system, particularly RS–I, and perform more realistic simulation analyses and experimental studies with a real HICE, or emulated exhaust gas conditions, to confirm the present results.

Acknowledgements

The authors would like to thank Professor Dr. Sebastian Verhelst (Ghent University), Professor Dr. Toshio Shudo (Hokkaido University), and Mr. Norihira (Mazda Motor Corporation) for providing valuable information regarding HICE thermal behavior, and also thank Mr. Wolfgang Thiel (BMW Group) for the helpful information that he provided regarding the estimation of the amount of water from an HICE.

REFERENCES

[1] Ibaraki S, Endo T, Kojima Y, Takahashi K, Baba T, Kawajiri S. Study of efficient on-board waste heat recovery system using Rankine cycle. JSAE Paper No. 20074413, 2007.
[2] Ringler J, Seifert M, Guyotot V, Hubner W. Rankine cycle for waste heat recovery of IC engines. SAE Technical Paper No. 2009-01-0174, 2009.
[3] Verhelst S, Maesschalck P, Rombaut N, Sierens R. Efficiency comparison between hydrogen and gasoline, on a Bi-fuel hydrogen/gasoline engine. International Journal of Hydrogen Energy 2009;34(5):2504–10.
[4] Sugisita H, Mori H, Uematsu K. A study of thermodynamic cycle and system configurations of hydrogen combustion turbines. International Journal of Hydrogen Energy 1998; 23(8):705–12.
[5] Tang X, Kabat DM, Natkin RJ, Stockhausen WF, Heffel J. Ford P2000 hydrogen engine dynamometer development. SAE Technical Paper No. 2002-01-0242, 2002.

[6] Natkin RJ, Tang X, Whipple KM, Kabat DM, Stockhausen WF. Ford hydrogen engine laboratory testing facility. SAE Technical Paper No. 2002-01-0241, 2002.
[7] Ball M, Wietschel M. The future of hydrogen – opportunities and challenges. International Journal of Hydrogen Energy 2009;34(2):615–27.
[8] Guthrie BR. Hydrogen G-cycle rotary internal combustion engine, in United States Patent No. US2008/0247897 A1: 2008.
[9] White CM, Steeper RR, Lutz AE. The hydrogen-fueled internal combustion engine: a technical review. International Journal of Hydrogen Energy 2006;31(10):1292–305.
[10] Depcik C, http://www.depcik.com/eduprograms/aftp.htm; 2003.
[11] Furuhama S, Hiruma M, Enomoto Y. Development of a liquid hydrogen car. International Journal of Hydrogen Energy 1978;3(1):61–81.
[12] Zhou L, Liu X, Liu F, Sun B, Schock HJ. Backfire prediction in a manifold injection hydrogen internal combustion engine. International Journal of Hydrogen Energy 2008;33(14):3847–55. TMS07: Symposium on Materials in Clean Power Systems.
[13] Theil W, Hartmann K. Equations and methods for testing hydrogen fuel consumption using exhaust Emissions. SAE Technical Paper No. 2008-01-1036, 2008: pp. 1–9.
[14] Theil W, Hartmann K. Possible influences on fuel consumption calculations while using the hydrogen-balance method. SAE Technical Paper No. 2008-01-1037, 2008.
[15] Mazzetti MJ. Use of flow through capacitor in the recovery and purification of water from exhaust gases of internal combustion engines, in United States Patent No. US7000409B2: 2006.
[16] McQuiggan G., Myers GA, Chhabra N, Gaio G. Turbine exhaust water recovery system, in United States Patent No. US7194869B2: 2007.
[17] Vetrovec, J. Internal combustion engine/water source system, in United States Patent No. US7302795B2: 2007.
[18] Kahraman E, Cihangir OzcanlI S, Ozerdem B. An experimental study on performance and emission characteristics of a hydrogen fuelled spark ignition engine. International Journal of Hydrogen Energy 2007;32(12):2066–72.
[19] Heywood JB. Internal combustion engine fundamentals. In: Morriss JM, editor. McGraw-Hill, Inc.; 1988.
[20] Chammas RE, Clodic D. Combined cycle for hybrid vehicles. SAE Techical Paper No. 2005-01-1171, 2005.
[21] Pitts DR, Sissom LE. In: Gilson B, editor. Schaum's outline of theory and problems of heat transfer. 2nd ed. New York: McGraw-Hill, Inc.; 1997.
[22] Noie SH. Investigation of thermal performance of an air-to-air thermosyphon heat exchanger using ϵ-NTU method. Applied Thermal Engineering 2006;26(5–6):559–67.
[23] Sanaye S, Rezazadeh M. Transient thermal modelling of heat recovery steam generators in combined cycle power plants. International Journal of Energy Research 2007;31(11): 1047–63.
[24] Hounsham S, Stobart R, Cooke A, Childs P. Energy recovery systems for engines. SAE Technical Paper No. 2008-01-0309, 2008.
[25] Yüksel F, Ceviz MA. Thermal balance of a four stroke SI engine operating on hydrogen as a supplementary fuel. Energy 2003;28(11):1069–80.
[26] Lemmon EW, Huber ML, McLinden MO. Reference fluid thermodynamic and transport properties (REFPROP), Version 8.0. In: NIST standard reference database 23. Gaithersburg, MD: National Institute of Standards and Technology; 2007.
[27] Wallner T, et al. Fuel economy and emissions evaluation of BMW Hydrogen 7 mono-fuel demonstration vehicles. International Journal of Hydrogen Energy 2008;33(24):7607–18.
[28] Mohammadi A, Shioji M, Nakai Y, Ishikura W, Tabo E. Performance and combustion characteristics of a direct injection SI hydrogen engine. International Journal of Hydrogen Energy 2007;32(2):296–304.
[29] Verhelst S, Maesschalck P, Rombaut N, Sierens R. Increasing the power output of hydrogen internal combustion engines by means of supercharging and exhaust gas recirculation. International Journal of Hydrogen Energy 2009;34(10):4406–12. 2nd World Hydrogen Technologies Convention.
[30] Verhelst S, Sierens R. Aspects concerning the optimisation of a hydrogen fueled engine. International Journal of Hydrogen Energy 2001;26(9):981–5.
[31] Verhelst S, Sierens R. Hydrogen engine-specific properties. International Journal of Hydrogen Energy 2001;26(9):987–90.
[32] Wakayama N, Morimoto K, Kashiwagi A, Saito T. Development of hydrogen rotary engine vehicle. In: 16th World Hydrogen Energy Conference (WHEC). 2006. Lyon France.
[33] Shudo T. Improving Thermal efficiency by reducing cooling losses in hydrogen combustion engines. International Journal of Hydrogen Energy 2007;32(17):4285–93.
[34] Shudo T, Nabetani S, Nakajima Y. Analysis of the degree of constant volume and cooling loss in a spark ignition engine fuelled with hydrogen. International Journal of Engine Research 2001;2(1):81–92.